A mathematical model for prediction of long-term degradation effects in solid oxide fuel cells

Authors:

Mina Naeini, Haoxiang Lai, James S. Cotton, Thomas A. Adams II

Date Submitted: 2021-06-15

Keywords: sulfur poisoning, electrolyte degradation, anode degradation, pore size degradation, nickel coarsening, Solid Oxide Fuel Cells

Abstract:

A mathematical model of long-term solid oxide fuel cell (SOFC) degradation is proposed, based on a cross-cutting meta-study of SOFC degradation research available in the open literature. This model is able to predict long-term SOFC performance under different operating conditions, and it accounts for the main degradation mechanisms, including: Ni coarsening and oxidation; anode pore size changes; degradation of anode and electrolyte conductivity; and sulfur poisoning. The results of the study indicate that SOFCs initially degrade quickly, but that the degradation rate diminishes significantly after approximately 1200 hours of operation. Consequently, the effects of different factors associated with degradation rate are investigated, including current density, temperature, and partial pressure of H2 in fuel source. Sensitivity analyses show that current density and H2 partial pressure have the highest and the lowest impact, respectively. In addition, the model has been developed to assess sulfur poisoning within pre-reformed hydrocarbon-fuel-based SOFCs. While previous models have mostly focused on performance loss in H2-fueled SOFCs. H2S deactivates catalytic activity of the SOFCs by reducing electrochemical activity and hydrocarbon conversion. Therefore, sulfur affects SOFCs that use different fuel sources in different ways. As a result, the models developed for H2-fueled SOFCs cannot be used for hydrocarbon-fueled ones.

Record Type: Preprint

Submitted To: LAPSE (Living Archive for Process Systems Engineering)

Citation (overall record, always the latest version):	LAPSE:2021.0525
Citation (this specific file, latest version):	LAPSE:2021.0525-1
Citation (this specific file, this version):	LAPSE:2021.0525-1v1

DOI of Published Version: https://doi.org/10.1021/acs.iecr.0c05302

A Mathematical Model for Prediction of Long-Term Degradation Effects in Solid Oxide Fuel Cells

Mina Naeini[1], Haoxiang Lai[1], James S. Cotton[2], Thomas A. Adams II[1]*

[1]Department of Chemical Engineering, McMaster University

[2]Department of Mechanical Engineering, McMaster University

* Corresponding author: tadams@mcmaster.ca

Keywords

Solid oxide fuel cells, nickel coarsening, nickel oxidation, pore size degradation, anode degradation, electrolyte degradation, sulfur poisoning.

Abstract

A mathematical model of long-term solid oxide fuel cell (SOFC) degradation is proposed, based on a cross-cutting meta-study of SOFC degradation research available in the open literature. This model is able to predict long-term SOFC performance under different operating conditions, and it accounts for the main degradation mechanisms, including: Ni coarsening and oxidation; anode pore size changes; degradation of anode and electrolyte conductivity; and sulfur poisoning. The results of the study indicate that SOFCs initially degrade quickly, but that the degradation rate diminishes significantly after approximately 1200 hours of operation. Consequently, the effects of different factors associated with degradation rate are investigated, including current density, temperature, and partial pressure of H_2 in fuel source. Sensitivity analyses show that current density and H_2 partial pressure have the highest and the lowest impact, respectively. In addition, the model has been developed to assess sulfur poisoning within pre-reformed hydrocarbon-fuel-based SOFCs. While previous models have mostly focused on performance loss in H_2-fueled SOFCs. H_2S deactivates catalytic activity of the SOFCs by reducing electrochemical activity and hydrocarbon conversion. Therefore, sulfur affects SOFCs that use different fuel sources in different ways. As a result, the models developed for H_2-fueled SOFCs cannot be used for hydrocarbon-fueled ones.

Nomenclature

Nomenclature

A area, m^2

A_{opt} area of active TPB region, m^2

A_j^V volume-specific surface area of reaction j, $m^2\ m^{-3}$

c_i stoichiometric coefficient of species i

c'_j stoichiometric coefficient of species in forward reaction

c''_j stoichiometric coefficient of species in backward reaction

D_p pore diameter, m

D_w width of a corrugation, m

D_{YSZ} mean diameter of YSZ particles, m

D_{Ni} mean diameter of Ni particles, m

D_s atomic surface diffusion coefficient, $m^2\ s^{-1}$

D_{eff} effective diffusivity, $m^2\ s^{-1}$

$D_{i\text{-}j}$ binary diffusivity, $m^2\ s^{-1}$

D_k Knudsen diffusivity, $m^2\ s^{-1}$

E_{act} activation energy, $KJ\ mol^{-1}$

F Faraday's constant, $C\ mol^{-1}$

I current, A

i current density, $A\ cm^{-2}$

i_0 exchange current density, $A\ cm^{-2}$

k_B Boltzmann constant, $J\ K^{-1}$

L length, m

L' reaction-region thickness, m

M_i mean molar mass, $kg\ mol^{-1}$

N_{Ni} number of Ni particles

Greek Symbols

η overpotential loss, V

σ electrical conductivity, $\Omega^{-1}\ m^{-1}$

φ porosity

τ relaxation time, s

τ_s surface tortuosity

τ_l electrode tortuosity

ε volume fraction

β fitting parameter

λ fitting parameter

γ surface energy, $J\ m^{-2}$

γ_l pre-exponential factor in electrode, $A\ m^{-2}$

Ω volume element, m^3

δ_s thickness, m

α fraction of the reaction heat produced in the anode

v_i diffusion volume of species i

θ overlap angle, 15°

ρ_i density, $kg\ m^{-3}$

Subscripts and Superscripts

0 initial condition

ac air channel

an anode

ca cathode

ch channel

ele electrolyte

fc fuel channel

ic interconnect

ohm ohmic

n equivalent electron per mole of reactant, equiv mol^{-1}	act activation
P pressure, Pa	con concentration
Pr site occupation probability	t channel shoulder
R gas constant, J mol^{-1} K^{-1}	el electronic
R_i net rate of phase i formation, mol m^{-3} s^{-1}	io ionic
r average radius of particles, m	ref reference
rd degradation rate, % / 1000 hours	x x direction
$\dot{s}_{i,j}$ rate of formation of phase i in reaction j mol m^{-2} s^{-1} (for two-phase reactions) mol m^{-1} s^{-1} (for three-phase reactions)	y y direction
T temperature, K	z z direction
t time, s	pd product
TPB triple phase boundary	re reactant
ΔV_s voltage drop due to sulfur poisoning, V	
V voltage, V	
V_{Ni} volume of Ni phase, m^3	
W weighting factor	
$\overline{Z_0}$ average initial coordination number	

1. Introduction A solid oxide fuel cell (SOFC) is a power-generation unit that enables direct conversion of chemical energy from a fuel source into electrical energy with high electrical efficiency (60 $\%_{LHV}$). SOFC systems can be used at a wide variety of scales, such as in integrated community energy systems (ICEs) to supply heat and power at scales on the order of ten thousand people. Unlike other fuel cells that require H_2, SOFCs can generate electricity using various types of hydrocarbon-based fuels, including natural gas. The large amount of useful waste heat generated at high operating temperatures means that the heat can be harvested to further increase the total system level energy efficiency to 85%$_{LHV}$. For instance, this captured heat can be distributed via

hot water pipes to meet the community's heat demands [1]. This is a key feature of SOFCs when integrated in ICEs, as replacing typical gas boilers with SOFCs can significantly reduce a community's GHG emissions. However, the limited lifetime of SOFCs has prevented their large-scale commercialization. In addition, it is critical to determine the proper cell size when implementing SOFCs in an ICE, as this will ensure that the community's energy needs are met. Furthermore, the loss in performance over time makes it important to determine not only the SOFC's initial performance capabilities, but also what its power output will be after long-term operation, as this information is critical for sizing and operating decisions [2].

The key to increasing lifetime of the SOFCs is to understand the various physical, chemical, and electrochemical reactions that take place by contaminants in the gas feed and operating conditions of SOFCs [3,4]. Deterioration processes affect various characteristics of the cells, such as the number and size of nickel particles, anode pore size and conductivity, the density of the triple phase boundary (TPB), and electrolyte conductivity [4]. A good degradation model should enable the rate and magnitude of irreversible performance loss to be measured at particular operating conditions, and it should also enable the determination of the cell's optimal operating conditions, thus extending its lifetime. Once these specifications have been identified, it is then possible to calculate which size of SOFC is ideal for an ICE under the given conditions. Although several studies have explored SOFC degradation, a general model that accounts for degradation mechanisms in the literature is still lacking. Due to several assumptions, the previously proposed models underestimate the degradation rate, which leads to the unrealistic sizing of the system [3–7]. Operating conditions such as temperature and current density significantly impact the long-term performance of SOFCs [3]; hence, the development of a degradation model that can account for effect of these parameters would allow system designers to change the design or the way it is operated in order to increase the lifetime of the cells [3]. Although the SOFC's high operating temperature affects the electrochemical reactions and the chemical stability of its components, it is not clear whether the SOFC's lifespan would be enhanced if it were run at lower temperatures. While some studies have found a positive correlation between degradation rate and temperature [8–11], others have shown that the degradation rate actually increases at lower temperatures [9,12,13]. Degradation mechanisms that occur due to interdiffusion, decomposition, corrosion of materials, or agglomeration of particles are more severe at higher temperatures, while poisoning-based processes such as sulfur poisoning are more prominent at lower temperatures [11]. Although

poisoning and contamination are highly deteriorative, they can usually be avoided or controlled by coating SOFC components or changing their microstructure, or by changing fuel composition or the stoichiometry ratio [14–20]. Experiments studying the poisoning of SOFC components are usually performed under accelerated contamination conditions or on symmetric cells rather than full cells. Moreover, these experiments often focus on the isolated effects of contaminants, which means that their results do not account for the complex interactions between deterioration reactions across a full SOFC [12,13]. Other studies have found that the effects of other degradation mechanisms can be decreased and controlled by varying operating parameters, though they cannot be completely avoided [4].

A summary of degradation models found in the literature can be found in Table 1. From this summary, it is clear that the effects of operating temperature on SOFC performance are not very straightforward. For example, Nakajo et al.'s data-driven model and Parhizkar's model show that SOFCs have longer lifetimes when operated at lower temperatures [4,10]. The model developed by Nakajo et al. accounts for deterioration processes such as Ni particle coarsening in the anode, reduced electrolyte conductivity, and the corrosion of interconnect material [10]. Parhizkar et al.'s model considers Ni coarsening and oxidation, and anode conductivity degradation [4]. In contrast, Yoshizumi et al. found sulfur poisoning to be the main SOFC degradation mechanism, and performance loss increased at lower temperatures due to sulfur contamination [21].

Table 1. Overview of different models for SOFC performance.

Ref.	Notes	Common system degradation mechanisms in conventional SOFCs						Other phenomena considered	Degradation correlation with temperature
		Ni coarsening	Ni oxidation	Changes in anode pore size	Changes in anode electrical conductivity	Changes in electrolyte ionic conductivity	Sulfur poisoning		
Zaccaria et al. [3]	An algebraic equation for degradation rate is found by fitting to the experimental data.								Negative correlation
Parhizkar et al. [4]		✓	✓		✓				Positive correlation
Larrain et al. [22]								Interconnect degradation	Positive correlation
Nakajo et al. [23]		✓				✓		Zirconate formation in the LSM/YSZ cathode and anode re-oxidation. Cr poisoning.	Positive correlation
Aguiar et al. [7]	Provides an electrochemical model for SOFC that only accounts for inevitable degradation processes.								
Wen et al. [24]	Couples an electrochemical model with a thermodynamic model, but only accounts for inevitable degradation mechanisms.								Negative correlation
Yang et al. [6]	Develops an electrochemical model for SOFC that only accounts for inevitable losses.								
Ryan et al. [25]	Constructs a damage model for SOFC degradation using experimental plots and fitting methods.				✓		✓	Changes in TPB and anode electrical conductivity due to sulfur and antimony poisoning.	Negative correlation
Hansen [26]							✓		Negative correlation
Tucker et al. [27]	An algebraic equation for degradation rate is found by fitting to the experimental data.								

Nakajo et al. [10]		✓				✓		Interconnect corrosion, and Chromium contamination of cathode	Negative correlation
Yoshizumi et al. [21]							✓		Negative correlation
This Work		✓	✓	✓	✓	✓	✓		Positive correlation

As it can be seen in Table 1, some of the models developed for SOFC performance prediction only consider inevitable performance drop, which is a part of overpotential caused by unavoidable physical, chemical, and electrochemical deteriorating processes. Conventional thermodynamic equations for ohmic, activation, and concentration overpotentials account for inevitable performance losses (Eqs. 7-9, 32, 36, and 37 in the next section). However, system degradation processes can increase overpotential. Overpotential caused by system degradation mechanisms can be avoided or controlled by system design and operation [4]. To yield a precise prediction of long-term performance degradation in SOFCs, system losses should be added to the inevitable overpotentials. In other words, a comprehensive degradation model should account for the overpotentials due to system degradation mechanisms (such as deterioration of anode microstructure, degradation of anode and electrolyte conductivities, and contamination of the cells) in addition to the inevitable overpotentials. Most of the system deterioration reactions that are common in the conventional SOFCs are listed in columns 3-8 of Table 1. All models for SOFC performance degradation take inevitable overpotentials into account. But these models usually ignore most system losses for simplification.

1.1 System degradation mechanisms

Several models have been developed for system contamination and degradation mechanisms in SOFCs. Models employed in the proposed comprehensive SOFCs performance models in this work are discussed in the following subsections.

1.1.1 System degradation mechanisms in electrolyte

As modeled by Coors et al., yttria-stabilized zirconia (YSZ), which is the conventional electrolyte material for SOFCs, shows deterioration in electrical conductivity with time [28]. This is a system degradation mechanism that increases ohmic overpotential, however SOFC performance models usually assume that the electrical conductivity of YSZ does not change with time [4,7,24].

1.1.2 System degradation mechanisms in anode

Degradation of anode microstructure that occurs in the form of Ni coarsening and oxidation, and in the pore diameter is a common cause of performance loss in anode-supported SOFCs. The number of nickel particles in the Ni-cermet anode decreases due to coarsening and oxidation. Gao et al. have proposed a theoretical model for the coarsening of nickel particles under SOFC operating conditions [29], while Neidhardt et al. have developed a model for the oxidation of nickel particles due to the presence of oxygen and steam at high temperature [30].

In addition to these factors, it is also important for degradation models to consider other consequences of nickel coarsening and oxidization, such as changes in pore size, degradation of anode electrical conductivity, and changes in area of active regions. Hardjo et al. studied the degradation of anode electrical conductivity as a result of a decrease in the number of nickel particles and an increase in their size [31,32]. Although pore size is generally assumed to be constant in degradation models, changes in pore diameter over time can affect SOFC performance by altering the area of active regions, TPB density, and mass diffusivity at the anode [4,6,7,24]. The model by Divisek and Wilkenhoener was selected for calculation of anode pore size [33]. Then it was updated by the size of Ni particles after coarsening to measure the changes in the pore size.

Different methods have been proposed for avoiding or decreasing the effects of degradation mechanisms. For instance, it is possible to reduce or avoid some of the contaminating mechanisms

in SOFCs by changing or modifying its microstructure. In addition, selecting the proper carbon-to-steam molar ratio makes it possible to largely avoid carbon deposits on Ni-based anodes in hydrocarbon-fueled SOFCs [20]. Chromium poisoning of the cathodes also can be reduced significantly by applying proper coatings on the interconnect and the cathode [16]. Conversely, other studies have shown that the best approach to reducing sulfur poisoning is by controlling operating conditions, such as temperature and current density [13,20,25,34,35]. SOFCs have a high degree of fuel flexibility, which makes them suitable for use in ICEs, as they can be easily operated using natural gas (NG). However, NG contains H_2S, which can contaminate the SOFC's anode. This is problematic, as Aguilar et al. found sulfur contamination of the anode to be the main cause of cell performance degradation, with overall cell resistance increasing alongside the H_2S concentration [36].

Various researchers have also modeled sulfur poisoning of H_2-fueled SOFCs [25,26]. For instance, Ryan et al. developed a damage model to quantify SOFC performance loss due to sulfur contamination, with results showing that performance deterioration is more severe at lower temperatures and when the fuel contains higher concentrations of H_2S [25]. Prior sulfur poisoning models account for the impact of temperature on sulfur contamination in SOFC anodes that are supplied with H_2. Other research has found that current density also affects sulfur poisoning in Ni-YSZ anodes, as oxygen ion concentration changes with current density [35].

Unfortunately, the developed sulfur-poisoning models for H_2-fueled anodes cannot be used for hydrocarbon-fueled SOFCs. This lack of transferability is due to the fact that H_2S not only poisons electrochemical reactions in the presence of hydrocarbons, but it also reduces catalytic reactions such as internal methane reformation [25,35]. Studies have shown that sulfur contamination of the SOFC anode can mostly be avoided by removing H_2S from the fuel stream [21,35,37]. For example, Yoshizumi et al. showed that injecting a desulfurized fuel into an anode that has previously been poisoned by sulfur will cause sulfur desorption from the anode surface, reversing the sulfur poisoning effects. [21]. However, recovering from the effects of sulfur contamination requires sulfur removal and gas sweetening operations upstream which, depending on the scale of the system and intended application, may not always be practical. This would come at additional balance-of-plant costs, and more research is needed to examine the economic and practicality trade-offs with the context of SOFC degradation for hydrocarbon systems.

The models listed in Table 1 and discussed above face two main issues: 1) they ignore some of the main deteriorating mechanisms, and 2) an algebraic expression of degradation or voltage is produced by fitting to experimental data points, making the expression case-specific rather than generalizable. The objective of the present study is to develop a comprehensive model that accounts for the dominant degradation processes that commonly happen in SOFCs, primarily via theoretical equations. The proposed model accounts for the following degradation mechanisms: a) Ni coarsening, b) Ni oxidation, c) changes in anode pore size, d) changes in anode electrical conductivity, e) changes in electrolyte ionic conductivity, and f) sulfur poisoning. These are most of the common deterioration processes in conventional SOFCs with Ni-YSZ anodes, YSZ electrolytes, and $La_{1-x}Sr_xMnO_3$ (LSM) cathodes. Although different models are developed for each of these mechanisms in the literature, to the best of authors' knowledge this is the first model that takes all of these into account holistically and can be used for a broad range of applications. In the previously proposed models, most of these mechanisms have been ignored for simplification which results in underestimation of SOFCs degradation over long period of time.

The proposed model considers the common degradation effects to simulate the impact of operating conditions on long-term performance of SOFCs, thus allowing it to provide realistic results requiring minimal assumptions. The model applies to both hydrogen and hydrocarbon fuels, because it is informed by data from current density impact studies by Hagen et al [35]. The results of this research are important for the wide commercialization of SOFCs in ICEs, as the presented model will allow system designers to select the optimal ICE system design and operational parameters with the degradation rate integrated into the control and operation strategy. Not only will this increase the SOFC's lifetime, but it will also allow system designers to select the optimal cell size for their specific energy system.

2. Modeling approach

An SOFC consists of a porous anode and cathode, dense electrolytes, and a metallic interconnect. The cell works by reducing oxygen molecules at the cathode/electrolyte interface to form oxygen ions which then migrate through the electrolytes to the anode. Once at the anode, the ions oxidize the fuel source via an electrochemical reaction (Eq. 1), producing high-temperature steam and free electrons.

$$H_2 + O^{2-} \rightarrow H_2O + 2\ e^- \quad (1)$$

Dense YSZ, which is the electrolyte conventionally used in SOFCs, prevents direct fuel combustion via the solid-state conduction of ions. YSZ has a selective diffusion property, which allows the conduction of oxygen ions, but prevents the transport of gases molecules [38]. Moreover, YSZ's low electrical conductivity ensures the transfer of free electrons through the external circuit connecting the anode and the cathode, resulting in the generation of electricity (Fig. 1). Electrochemical reactions occur at the triple phase boundary (TPB), which is the interface between gas, the electrode, and the electrolyte.

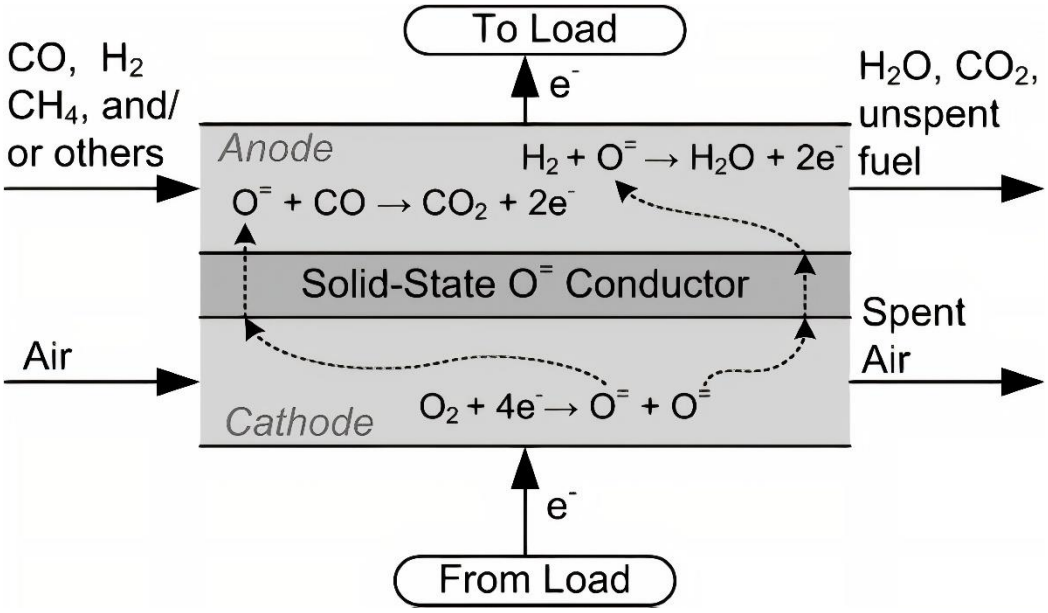

Fig. 1. Schematic of SOFC operation. Reprinted with permission from [39]. Copyright (2013) American Chemical Society.

The maximum voltage of an SOFC is achieved in an open circuit condition and is known as open circuit voltage (OCV). OCV can be calculated at different temperatures and partial gas pressures via the Nernst Equation (Eq. 4) and the Gibbs free energy change from the SOFC reaction, as shown in Eq. 2 [40].

$$\Delta G = \Delta G^{\circ} - \mathrm{R}T \ln\left(\frac{P_{\mathrm{H_2}} \cdot {P_{\mathrm{O_2}}}^{1/2}}{P_{\mathrm{H_2O}}}\right) \quad (2)$$

In Eq. 2, ΔG° is the Gibbs free energy change of the water formation reaction (Eq. 1) at standard pressure (1 atm), and P_i is the partial pressure of gas species i in the fuel and air channels.

$$E = \frac{-\Delta G}{n\mathrm{F}} \tag{3}$$

Where E is the OCV at the SOFC's operating condition, n is the moles of electrons involved in the water formation reaction, (2 for Eq. 1), and F is the Faraday constant. The Nernst Equation is then obtained by substituting Eq. 2 into Eq. 3:

$$E = E^{\circ} + \frac{\mathrm{R}T}{n\mathrm{F}} \ln\left(\frac{P_{\mathrm{H_2}} \cdot {P_{\mathrm{O_2}}}^{1/2}}{P_{\mathrm{H_2O}}}\right) \tag{4}$$

In this equation, E° is the SOFC's OCV at standard pressure (1 atm).

In addition, the OCV for SOFCs that use other types of fuels can be calculated using the Nernst equation with the Gibbs free energy change of the fuel's oxidation reaction. Eq. 5 shows the general form of OCV for fuel's oxidation reaction:

$$E = E^{\circ} + \frac{\mathrm{R}T}{n\mathrm{F}} \ln\left(\frac{\prod_{re} P_{re}^{c_{re}}}{\prod_{pd} P_{pd}^{c_{pd}}}\right) \tag{5}$$

Where re and pd stand for reactants and products, respectively. P_{re} and P_{pd} are partial pressure of reactants and products. While, c_{re} and c_{pd} account for the stoichiometric coefficients of reactants and products in the fuel's oxidation reaction, respectively.

When current flows through the external circuit, voltage deviates from the OCV due to activation, ohmic, and concentration overpotentials/polarizations (Eq. 6) [7,40]. Overpotentials partially occur as a result of physical, chemical, and electrochemical reactions in the cell components; the rest of the potential loss is caused by degradation mechanisms, which can be reduced or controlled by varying the cell's operating parameters [4]:

$$V(t) = E - (\sum_k \eta_{\mathrm{ohm,k}}(t) + \eta_{\mathrm{act,an}}(t) + \eta_{\mathrm{act,ca}}(t) + \eta_{\mathrm{con,an}}(t) + \eta_{\mathrm{con,ca}}(t)) \tag{6}$$

where η_{ohm} is the ohmic losses from electronic and ionic resistances in or between cell compartments (k = anode, cathode, electrolyte, and interconnect), $\eta_{\mathrm{act,an}}$ and $\eta_{\mathrm{act,ca}}$ are the activation overpotentials that are needed to overcome energy barriers of electrochemical reactions in the anode and cathode respectively, and $\eta_{\mathrm{con,an}}$ and $\eta_{\mathrm{con,ca}}$ are concentration overpotentials due to the spatial gradient of gases concentration in the anode and cathode, respectively. Overpotentials are caused due to inevitable losses and system degradation mechanisms. Conventional

thermodynamic equations for overpotentials only account for inevitable losses. To consider system losses, relative models of degradation mechanism should be implemented into/added to thermodynamic equations.

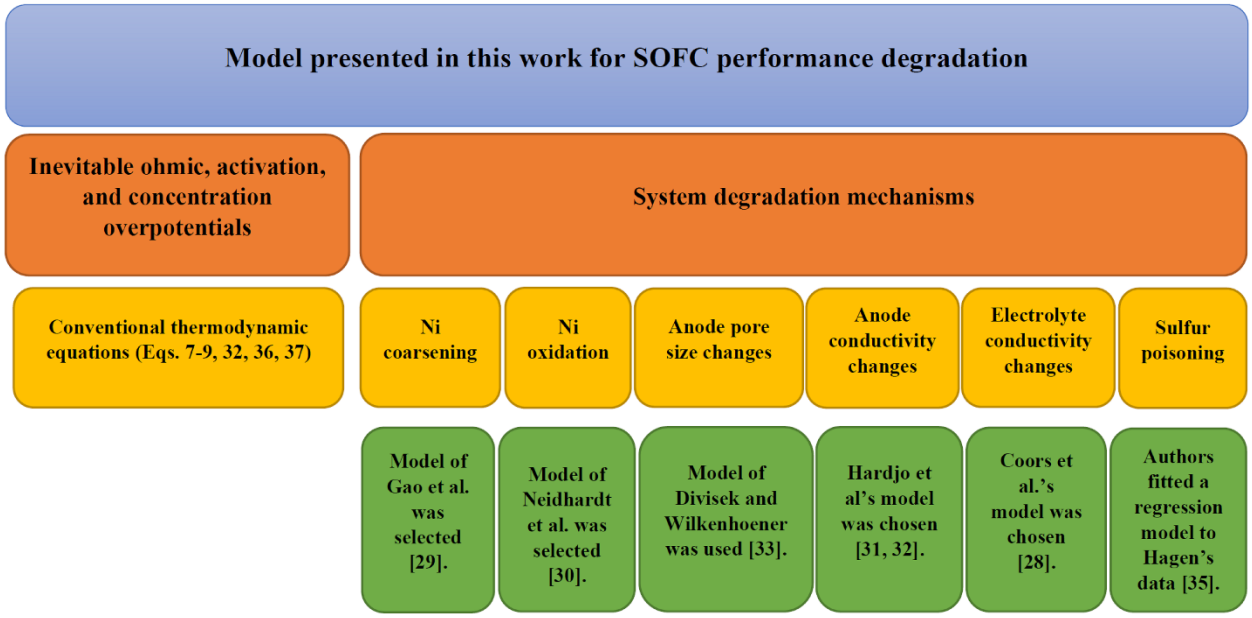

Fig. 2. Outline of the SOFC long-term performance model in the present study.

For some of the degradation mechanisms, different models have been presented in the literature. In this work, in order to find the best model for each phenomenon, the models were validated against experimental data. Those that showed the best agreement with experiments were used in the current model and reported in the following sections.

2.1 Ohmic polarization

Ohmic overpotential is the result of ionic and electronic resistances within or between components. Ohmic losses in different components can be calculated via Ohm's Law [7,24].

$$\eta_{\mathrm{ohm,ic}} = I\left(\frac{L_{\mathrm{ic}}}{L_y L_z \sigma_{\mathrm{ic}}} + \frac{L_{\mathrm{fc}}}{(1+n_{\mathrm{ch}})L_t L_y \sigma_{\mathrm{ic}}} + \frac{L_{\mathrm{ac}}}{(1+n_{\mathrm{ch}})L_t L_z \sigma_{\mathrm{ic}}}\right) \quad (7)$$

$$\eta_{\mathrm{ohm,ele}} = I\left(\frac{L_{\mathrm{ele}}}{L_y L_z \sigma_{\mathrm{ele}}(t)}\right) \quad (8)$$

$$\eta_{\mathrm{ohm,l}} = I\left(\frac{\left(A_{\mathrm{opt},l}(t) - L_y L_z\right) L'_{\mathrm{opt},l}}{2\,A_{\mathrm{opt},l}(t)\,L_y L_z\,(1-\varphi_l)\sigma_{\mathrm{ele}}(t)} + \frac{L_l - L'_{\mathrm{opt},l}}{L_y L_z\,(1-1.8\varphi_l)\,\sigma_l(t)}\right) \quad (9)$$

$l = \mathrm{anode, cathode}$

Where I is the working current (A), L is the thickness (m), n_{ch} is the number of channels on electrode, σ_l is the conductivity of component l (Ω^{-1} m^{-1}), and $A_{opt,l}$ is the area of active TPB regions, which can be expressed as:

$$A_{opt,l}\,(t) = \left(1 + 2\frac{L'_{\mathrm{opt},l}}{D_{p,l}}\right) L_y\, L_z \tag{10}$$

In Eq. 10 L'_{opt} is the active TPB region thickness (m), and D_p is the average pore diameter (m). It can be assumed that cathode has parallel pores with average diameters that do not change over time, as cathodes are made from ceramic material that features high stability under oxidizing conditions (Eq. 11) [24].

$$D_{p,\mathrm{ca}} = D_{w,\mathrm{ca}}\,\varphi_{\mathrm{ca}}/(1 - \varphi_{\mathrm{ca}}) \tag{11}$$

$D_{w,\mathrm{ca}}$ is width of a corrugation in the cathode structure and φ_{ca} is the cathode porosity.

However, a more accurate model is required to capture the changes in the average diameter of anode pores that take place over time due to the oxidation and coarsening of Ni particles. Eq. 12 can be used to calculate anode pore size, as it accounts for the volume fraction and size of nickel particles that change over time [33].

$$D_{p,\mathrm{an}}(t) = D_{\mathrm{YSZ}}\,\varepsilon_{\mathrm{YSZ}}(t) + D_{\mathrm{Ni}}(t)\,\varepsilon_{\mathrm{Ni}}(t) \tag{12}$$

D_j is the average diameter of phase j particles (m), and ε_j is the volume fraction of phase j [6].

2.1.1 Nickel coarsening and Nickel oxidation

The size and number of Ni particles, as well as the volume fraction of solid phases in the Ni-cermet anode, change due to the agglomeration and oxidation of the Ni particles. Gao et al. developed a theoretical model for Ni coarsening [29], which showed that Ni particles initially show a rapid growth rate, but that this growth rate slows with time. The presence of YSZ in the anode microstructure prevents the extreme growth of Ni particles; thus, Ni particles reach a maximum radius in the composite microstructure [41]. This theoretical model has a fitting parameter (β) for minor adjustments whose value has a small impact on the final results. The model was fitted to Tanasini et al's experimental data [42] and showed a good agreement with their data.

$$\frac{r^5_{\mathrm{Ni,max}} - r^5_{\mathrm{Ni}}(t)}{r^5_{\mathrm{Ni,max}} - r^5_{\mathrm{Ni},0}} = \exp\left(\frac{-5\,C}{r^5_{\mathrm{Ni,max}} - r^5_{\mathrm{Ni},0}}\,t\right) \tag{13}$$

$r_{\mathrm{Ni,max}}$ and C are given as follows,

$$r_{\mathrm{Ni,max}}\,(t) = \left(\frac{\varepsilon_{\mathrm{Ni}}\,(t)\,\overline{Z_0}\,(1+3\beta^2) + (1+\beta)^3}{(1+\beta)^3}\right)^{1/3} r_{\mathrm{Ni},0} \tag{14}$$

$$C = D_s\,\frac{\gamma\,\Omega\,\delta_s}{2\,k_B T}\,\frac{\beta}{(1-\beta^2)\,(1+\beta^2)^{0.5}\,(1+\beta)^3}\,\overline{Z_0}\,\frac{\varepsilon_{\mathrm{Ni}}(t)}{\frac{\varepsilon_{\mathrm{Ni}}(t)}{r_{\mathrm{Ni},0}} + \frac{\varepsilon_{\mathrm{Ni}}(t)}{r_{\mathrm{YSZ}}}} \tag{15}$$

where k_B is the Boltzmann constant, r_{Ni} and r_{YSZ} are Ni particle size and radius of YSZ particles in the Ni-YSZ anode, $r_{\mathrm{Ni},0}$ is the initial radius of Ni particle, D_s is the atomic surface diffusion coefficient, Ω is the volume element, γ is the surface energy , δ_s is the thickness, $\overline{Z_0}$ is the average initial coordination number, and β is the fitting parameter which is adjusted such that model best fits the experimental data using a minimize sum of square errors approach. β received the value 0.038 for the anode microstructure tested by Tanasini et al. [41] .

The number of Ni particles after agglomeration ($N_{\mathrm{Ni,c}}$) can be calculated using the total volume of Ni phase [42]:

$$V_{\mathrm{Ni}}(t) = V_{\mathrm{Ni},0} \tag{16}$$

$$N_{\mathrm{Ni}}(t)\,\frac{4}{3}\,\pi\,r_{\mathrm{Ni}}^3(t) = N_{\mathrm{Ni},0}\,\frac{4}{3}\,\pi\,r_{\mathrm{Ni},0}^3 \tag{17}$$

$$N_{\mathrm{Ni},c}\,(t) = \left(\frac{r_{\mathrm{Ni},0}}{r_{\mathrm{Ni}}(t)}\right)^3 N_{\mathrm{Ni},0} \tag{18}$$

$V_{\mathrm{Ni},0}$ and $N_{\mathrm{Ni},0}$ are initial volume of Ni phase (m^3) and initial number of Ni particles, respectively.

In addition, Ni can be oxidized with oxygen molecules (Eq. 19) or steam (Eq. 20) through a thermochemical reaction [30].

$$\mathrm{Ni} + \frac{1}{2}\,\mathrm{O_2} \leftrightarrow \mathrm{NiO} \tag{19}$$

$$\mathrm{Ni} + \mathrm{H_2O} \leftrightarrow \mathrm{NiO} + \mathrm{H_2} \tag{20}$$

In order to calculate number of remaining particles after oxidation, it is necessary to first calculate the rate of NiO formation. The model developed by Neidhardt et al. can be used to achieve this task [30,43].

$$N_{\mathrm{NiO}}(t) = \int R_{\mathrm{NiO}}\,dt \tag{21}$$

Where R_{NiO} is the rate of NiO formation (mol m^{-3} s^{-1}) and N_{NiO} is the number of NiO particles formed during the oxidation of the anode. Eqs. 22-26 are used to calculate rate of NiO formation. The found Eq. for NiO formation then will substitute for R_{NiO} in Eq. 21 to quantify number of NiO particles formed in the anode.

$$\frac{\partial(\rho_i \varepsilon_i)}{\partial t} = R_i M_i \tag{22}$$

ρ_i and M_i are the density and molar mass of species i, respectively.

$$R_i = \sum_j \dot{s}_{i,j} A_j^V \tag{23}$$

A_j^V is the volume-specific surface area of reaction j (m^2/m^3).

$$A_j^V = f\, A_0^V \exp(-50\, \varepsilon_{\mathrm{NiO}}) \tag{24}$$

$$f = 1 - |tanh(10^9 \varepsilon_{\mathrm{NiO}}) - tanh(10^9\, \varepsilon_{\mathrm{Ni}})| \tag{25}$$

Where $\dot{s}_{i,j}$ represents the rate of species i production in reaction j (mol m^{-2} s^{-1}), which can be evaluated using Eq. 26.

$$\dot{s}_i = c_i \left(k_f \prod_{j \epsilon R_f} a_j^{c'_j} - k_r \prod_{j \epsilon R_r} a_j^{c''_j}\right) \tag{26}$$

In this equation, k_f and k_r represent the forward and backward rate constants, with c_i as the stoichiometric coefficient of species i, and c'_j and c''_j as the stoichiometric coefficients of species i in forward and backward reactions, respectively.

Eq. 27 shows the number particles remaining after coarsening and oxidation.

$$N_{\mathrm{Ni}}(t) = N_{\mathrm{Ni},c}(t) - N_{\mathrm{NiO}}(t) \tag{27}$$

2.1.2 Electrical conductivity of anode

Microstructural changes in the anode due to Ni agglomeration and oxidation result in the degradation of TPB density and electrical conductivity. The anode has a percolated network that consists of YSZ and Ni phases. Percolation theory can be used to calculate the TPB density and electrical conductivity of the percolated network [8,32,44]:

$$A(t) = K_A N_{\mathrm{Ni}}(t) \times 4\pi\, r_{\mathrm{Ni}}^2(t) \tag{28}$$

$A(t)$ is the active surface area of the catalyst layer in the anode.

$$\frac{Pr(t)}{Pr_c} = \frac{A(t)}{A_0} \quad (29)$$

Pr and Pr_c are site occupation probability and site occupation at the percolation threshold, respectively.

The electrical conductivity of an anode drops rapidly during the first hours of operation, but levels off later. Deterioration in anode conductivity is correlated to the coarsening of Ni particles [32,45].

$$\sigma_{Ni}(t) = f_r\, \sigma_{0,\text{an}} \left(\frac{Pr(t) - Pr_c}{1 - Pr_c}\right)^{1.3} \frac{\varepsilon_{\text{Ni}}(t)}{\tau_s} \quad (30)$$

Where σ_0 represents bulk conductivity, with τ_s as surface tortuosity and f_r as the ratio of the resistance of a continuous film to the resistance of a sintered film ($\frac{R_{\text{film}}}{R_{\text{eff}}}$), which is a function of the particles' overlap angle (almost 0.575 at angle 15°) [32]. Among the few models that were proposed for the anode electrical conductivity in the literature, we found this model to best agree with the experimental data by Klemenso et al. [46] with an R^2 of 0.947. In addition, the calculated site occupation probability in this work, showed an R^2 of 0.99 with the Klemenso et al.'s data [46]. See Appendix for validation information.

2.1.3 Electrolyte conductivity

Research has shown an exponential drop in the ionic conductivity of the YSZ electrolytes, which has been modeled by Coors et al. as follows [28]:

$$\sigma(t) = (\sigma_i - \sigma_f) \exp(-t/\tau) + \sigma_i \quad (31)$$

In Eq. 31, σ_i is the initial or maximum ionic conductivity of the electrolytes, while σ_f represents their final conductivity and τ is the relaxation time.

2.2 Activation polarization

Activation polarization, which is defined as an overpotential above equilibrium, takes place in order to overcome the activation energy barrier that limits the electrochemical reaction in the fuel cell that generates current [47]. The following equation, which is obtained by solving the Butler-Volmer equation, is used to quantify the activation overpotential of an SOFC [24]. The length of the TPB regions plays an important role in activation overpotential, as less activation overpotential is required to produce a specific current when larger active regions are available [6]. In following

equation, the effect of TPB density on activation polarization is embedded in the exchange current density, i_0.

$$\eta_{\mathrm{act},l} = \frac{\mathrm{R}T}{\alpha n \mathrm{F}} \sinh^{-1}\left(\frac{i_l(t)}{2i_{0,l}}\right) \tag{32}$$

Where α is the charge transfer coefficient and equals 0.5, and n is the number of electrons transferred in the reaction and takes the value of 2 for the anodic reaction and 4 for the cathodic reaction. The term $i_{0,l}$ represents the exchange current density (A m^{-2}), and can be calculated for the cathode and anode using Eqs. 33 and 34, respectively [48].

$$i_{0,\mathrm{ca}} = \gamma_{\mathrm{ca}}\left(\frac{P_{\mathrm{O_2}}}{P_{\mathrm{ref}}}\right)^{0.25} \exp\left(-\frac{E_{\mathrm{act,ca}}}{\mathrm{R}T}\right) \tag{33}$$

$$i_{0,\mathrm{an}} = \gamma_{\mathrm{an}}\left(\frac{P_{\mathrm{H_2}}}{P_{\mathrm{ref}}}\right)\left(\frac{P_{\mathrm{H_2O}}}{P_{\mathrm{ref}}}\right) \exp\left(-\frac{E_{\mathrm{act,an}}}{\mathrm{R}T}\right) \tag{34}$$

The working current density of the electrodes can be expressed as [24]:

$$i_l(t) = \frac{I}{A'_{opt,l}(t)} \tag{35}$$

Where γ_l is the pre-exponential factor (A m^{-2}), $E_{\mathrm{act},l}$ is the activation energy of the electrode (kJ mol^{-1}), and P_{ref} is the reference pressure, which is set to the atmospheric pressure.

2.3 Concentration polarization

Concentration overpotential takes place when the concentration of the gaseous reactants at reaction sites is lower than the bulk concentration. In fact, a spatial concentration gradient is produced when the rate of consumption of a reactant is higher than the rate of diffusion, which leads to fuel cell voltage degradation. In open-circuit condition, the concentration of gaseous species in the pores of the electrodes is the same as bulk concentration; however, spatial variation in concentration evolves with current flow, with higher currents resulting in larger concentration gradients [7,49]. The following model is used to evaluate concentration overpotential in the electrodes of SOFCs. The TPB is considered as the electrochemical active region in which fuel cell reactions take place. H_2 and H_2O are on the anode side, and O_2 and N_2 are on the cathode side [7].

$$\eta_{\mathrm{con,ca}} = \frac{\mathrm{R}T}{n\mathrm{F}} \ln\left(\frac{P_{\mathrm{O_2}}}{P_{\mathrm{O_2,TPB}}(t)}\right) \tag{36}$$

$$\eta_{\mathrm{con,an}} = \frac{\mathrm{R}T}{n\mathrm{F}} \ln\left(\frac{P_{\mathrm{H_2O,TPB}}\,(t)\,P_{\mathrm{H_2}}}{P_{\mathrm{H_2,TPB}}(t)\,P_{\mathrm{H_2O}}}\right) \tag{37}$$

The partial pressures of gaseous species at the TPB is a function of effective diffusivity at the electrode. Neglecting external diffusion, the partial pressures of gases at the TPB regions are given by [7,24]:

$$P_{\mathrm{H_2,TPB}}(T) = P_{\mathrm{H_2}} - \frac{\mathrm{R}T\,L_{\mathrm{an}}\,I}{n\,\mathrm{F}\,L_y\,L_z\,D_{\mathrm{eff,an}}(t)} \tag{38}$$

$$P_{\mathrm{H_2O,TPB}}(T) = P_{\mathrm{H_2O}} + \frac{\mathrm{R}T\,L_{\mathrm{an}}\,I}{n\,\mathrm{F}\,L_y\,L_z\,D_{\mathrm{eff,an}}(t)} \tag{39}$$

$$P_{\mathrm{O_2,TPB}}(t) = P_{\mathrm{air}} - \left(P_{\mathrm{air}} - P_{\mathrm{O_2}}\right)\exp\left(\frac{\mathrm{R}T\,L_{\mathrm{ca}}\,I}{n\,\mathrm{F}\,L_y\,L_z\,D_{\mathrm{eff,ca}}(t)\,P_{\mathrm{air}}}\right) \tag{40}$$

$$D_{\mathrm{eff,an}}(t) = \left(\frac{P_{\mathrm{H_2}}}{P_{\mathrm{f}}}\right) D_{\mathrm{H_2O,eff}}(t) + \left(\frac{P_{\mathrm{H_2O}}}{P_{\mathrm{f}}}\right) D_{\mathrm{H_2,eff}}(t) \tag{41}$$

$$D_{\mathrm{eff,ca}}(t) = D_{\mathrm{O_2,eff}}(t) \tag{42}$$

Where $D_{\mathrm{eff},l}$ is the effective diffusivity of the electrode ($m^2\ s^{-1}$).

Depending on the mean size of the pores and the mean free path of the gas molecules, Knudsen or binary diffusion can take place in porous structures. Binary diffusion occurs when gas molecules diffuse through pores that are larger than the mean free path of gas particles, while Knudsen diffusion occurs when the pores are smaller than the mean free path of the molecules [49].

The effective diffusion of gases in the porous electrodes of SOFCs is generally considered as a combination of Knudsen ($D_{i,K}$) and binary diffusion (D_{i-j}) to account for different porous structures [6].

$$D_{\mathrm{H_2,eff}}(t) = \frac{\varphi_{\mathrm{an}}}{\tau_{\mathrm{an}}}\left(\frac{1}{D_{\mathrm{H_2-H_2O}}} + \frac{1}{D_{\mathrm{H_2},K}(t)}\right)^{-1} \tag{43}$$

$$D_{\mathrm{H_2O,eff}}(t) = \frac{\varphi_{\mathrm{an}}}{\tau_{\mathrm{an}}}\left(\frac{1}{D_{\mathrm{H_2-H_2O}}} + \frac{1}{D_{\mathrm{H_2O},K}(t)}\right)^{-1} \tag{44}$$

$$D_{\mathrm{O_2,eff}}(t) = \frac{\varphi_{\mathrm{ca}}}{\tau_{\mathrm{ca}}}\left(\frac{1}{D_{\mathrm{O_2-N_2}}} + \frac{1}{D_{\mathrm{O_2},K}(t)}\right)^{-1} \tag{45}$$

Chapman et al. [50], Arnold [51], Gilliland [52], and Fuller et al. [53] have all developed different empirical models for binary gas diffusion. However, Fuller et al.'s semi-empirical method provides the best agreement with experimental results. Their model is expressed as follows [53]:

$$D_{i-j} = \frac{0.00143\, T^{1.75}}{P\, M_{ij}^{0.5}\, [(\sum \nu)_i^{\frac{1}{3}} + (\sum \nu)_j^{\frac{1}{3}}]^2} \quad (46)$$

T and P are the temperature and total pressure of the gas stream, respectively, while ν_i is the diffusion volume of species i (ν_{H_2} = 6.12, ν_{H_2O} = 13.1, ν_{O_2} = 16.3 and ν_{N_2} = 18.5). M_{ij} is defined as,

$$M_{ij} = 2[\frac{1}{M_i} + \frac{1}{M_j}]^{-1} \quad (47)$$

Where M_i is the molecular weight of species i in kg/mol.

Knudsen diffusion can be calculated using following equation:

$$D_{i,K}(t) = 48.5\, D_{p,l}(t)(\frac{T}{M_i})^{0.5} \quad (48)$$

2.4 Sulfur Poisoning

Sulfur poisoning takes place when fuel containing H_2S is supplied to the SOFC anode. This is commonly added as an odorant to hydrocarbon-based fuels, such as natural gas. The sulfur in the fuel is chemisorbed on the Ni-based anode at the SOFC's operating conditions, resulting in the deactivation of the anode's catalytic behavior [20,34]. A study by Matsuzaki and Yasuda showed that, at 750℃ and an H_2S concentration as low as 0.05 ppm, anode electrochemical performance deteriorates dramatically [54].

The key to SOFCs' fuel flexibility is their ability to convert hydrocarbons at high operating temperatures. Sulfur poisoning affects hydrocarbon conversion and electrochemical reactions. Prior findings have shown that, when the fuel stream contains 50 ppm H_2S, a large amount of the CH_4 supplied to the anode leaves the cell without being converted [55]. Different empirical models have been developed using curve-fitting approaches in order to show how sulfur contamination affects the performance of SOFCs. Alstrup applied a Temkin-like isotherm to explain sulfur adsorption on the Ni catalyst [56]. While a model developed by Hansen et al. illustrates a linear relationship between sulfur surface coverage and a drop in SOFC performance. This model was

obtained by fitting the experimental data obtained by Zha et al. and Cheng et al. for SOFC power loss with regards to surface coverage [26,57,58]. Ryan et al. used Zha et al.'s data to construct a damage model that shows the effects of sulfur poisoning on performance loss over a range of temperatures and H_2S concentrations [25,57].

The complex nature of sulfur poisoning is not well understood, as it depends on several factors, such as temperature, H_2S concentration, current density, and steam-to-carbon ratio [34,35,57]. Without considering these factors, models are confined to the operating conditions reported by Zha et al. for H_2-fueled SOFCs.

Studies have illustrated that impact of sulfur compounds on the catalytic activity of the Ni-based anodes occurs very rapidly that the time dependency of it can be neglected comparing to the long lifetime of the SOFCs [26]. In the present work, Hagen et al.'s experimental data is adapted to enable the model to be capable of simulating changes in SOFC performance with respect to current density at different H_2S concentrations [35]. The experimental data used in this model was obtained from a cell supplied with a fuel stream of 29% CH_4, 58% H_2O, and 13% H_2 mixed with various amounts of H_2S. This fuel mixture is a good representative of pre-reformed CH_4-containing fuel. Accumulated voltage drop versus H_2S concentration plots were given at 4 different current densities (0, 0.25, 0.5 and 1 A/cm^2). Using the given information at 0, 0.5 and, 1 A/cm^2, performance loss was modeled as a function of H_2S concentration and current density.

Thus, the following equations are suggested based on the cell's behaviour over the studied range of H_2S concentrations and current densities:

$$\Delta V_s = W_1 f_1\left(i, C_{H_2S}\right) + W_2 f_2\left(i, C_{H_2S}\right) \quad (49)$$

where ΔV_s is the voltage drop due to sulfur poisoning (V), with i as the current density (A/cm^2) and C_{H_2S} as the H_2S concentration in the fuel source (ppm).

When the model was fitted to Zha et al.'s experimental data, the functions of coefficients A and B were found to be;

$$f_1\left(i, C_{H_2S}\right) = \ln(C_{H_2S}) \quad (50)$$

$$f_2\left(i, C_{H_2S}\right) = Y_{max}(i)(1 - A_1(i) \exp\left(-A_2(i) \times C_{H_2S}\right)) \quad (51)$$

As shown in Figure 3, model replicates the shape of the experimental data by considering the weighted sum of two different functions with logarithmic or asymptotic behaviour. Each function

has a different weighting at different current densities. The weighting factors, W_1 and W_2, and other coefficients are given as follows:

$$W_1 = -0.039\, i^2 + 0.009\, i + 0.030 \quad (52)$$

$$W_2 = 1 - W_1 \quad (53)$$

$$A_1 = 0.827 \exp(0.411\, i) \quad (54)$$

$$A_2 = 0.064 \exp(0.995\, i) \quad (55)$$

SOFC performance declines as H_2S concentration increases until a monolayer of sulfur forms on the Ni-cermet anode. At this point, the anode reaches a saturation point after which the addition of more H_2S no longer significantly inhibits SOFC performance [26]. The saturation point depends on the current density, with higher current densities resulting in a greater loss in performance prior to reaching it. $Y_{\max}$ in Eq. 51 corresponds to the maximum performance loss (V), which is obtained under saturation conditions. Comparing the plots reported by Hagen et al. [35], it can be concluded that saturated performance loss is exponentially correlated with current density. Eq. 55 had the best agreement with the experimental data.

$$Y_{\max} = 6.749 \exp(1.559\, i) \quad (56)$$

The values of the coefficients were then calculated at 0.25 A/cm^2 to predict the accumulated voltage loss of the same cell obtained by the model (Fig. 3). An R^2 of 0.976 demonstrates the model's ability to predict the decline in SOFC performance due to the sulfur contamination when H_2S enters the cell with a pre-reformed hydrocarbon-based fuel mixture.

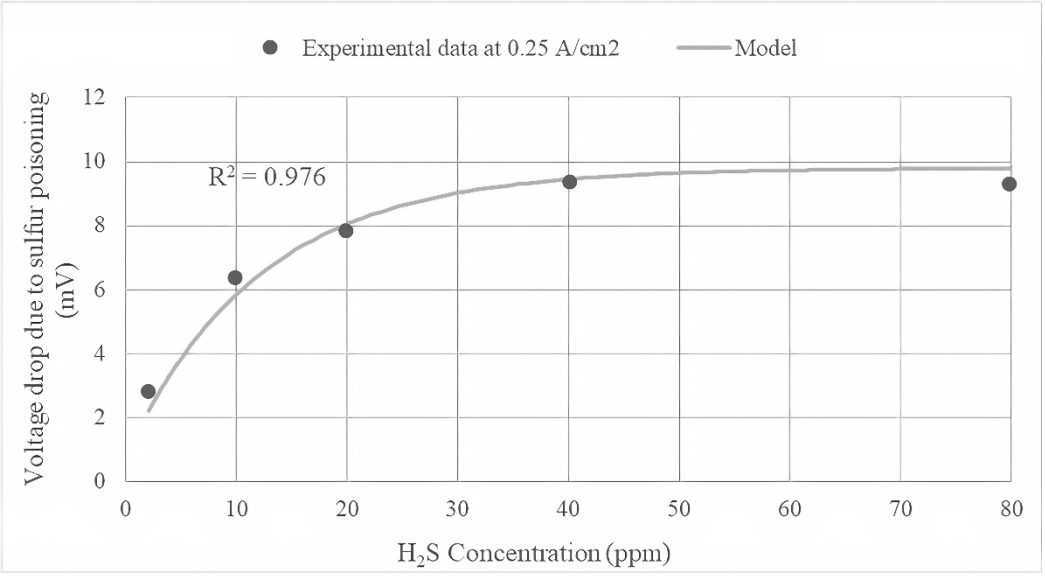

Fig. 3. Voltage drop due to sulfur poisoning versus H_2S concentration at 0.25 A/cm^2. The solid line shows the results of the proposed empirical model, while the circles represent Hagen et al.'s experimental data [35].

2.5 Degradation rate evaluation

Very different values have been reported for the degradation rate of conventional SOFCs in the literature [3,8,59,60]. There are several causes as to why the values reported for SOFC degradation rates are very different. Some possible reasons are that the components have microstructural differences from study to study which could be due to component composition or structure, cell design, testing condition, or fuel composition. However, one important cause of these differences is inconsistent definitions of the degradation rate itself. Eqs. 57 and 58 that have been used by Hagen et al. [59] and Gemmen et al. [60], respectively are two examples of degradation rate models in the literature.

$$rd(t) = \frac{OCV - V_t}{t} \times 1000 \tag{57}$$

$$rd(t) = \frac{V_i - V_t}{V_i \times (t - t_i)} \times 100 \tag{58}$$

where rd is the degradation rate, with V_i as initial voltage in the testing range and V_t as voltage at time *t*. These equations calculate rd over a long time period using backward finite differences with large timesteps (at least several hundred hours). The timesteps used in these equations are inconsistent. Eq. 58 defines degradation rate as voltage percentage change that happens over a specific time range with respect to the initial voltage of that range, while Eq. 57 measures degradation rate as absolute change in voltage from OCV and then normalized to 1000 hours. The unit of rd in Eq. 57 is V/1000h whereas that of Eq. 58 is %/h. Therefore, not only the differences in cell microstructure and experiment methodologies but inconsistent definitions make degradation rate values incomparable. To solve this problem, instantaneous rd should be computed (Eq. 59) instead of using different approximations of finite differences with inconsistent, large timesteps.

$$rd(t) = \frac{1}{V_i} \times \frac{dV_t}{dt} \tag{59}$$

The instantaneous rd is preferable for modeling because models are smooth and noiseless, and it can be consistently and unambiguously applied everywhere. We note that this definition cannot be

applied directly to experimental data due to the noise involved, but it can be approximated numerically through a centred finite differences approach with a relatively short timestep (a few hours), or though a local line fitting approach, depending on the noise.

2.6 Model Implementation

The model was implemented in MATLB. In order to calculate cell voltage at specific operating conditions, ohmic, activation and concentration polarizations should be calculated and implemented in Eq. 6. Eqs. 10-31 were utilized to find the impacts of various phenomena on ohmic losses in the cell components. These equations were then incorporated into Eqs. 7-9 to quantify ohmic polarization. In this section, ODE45 was used to compute the rate of nickel oxidation reaction (Eq. 25). Then, Eqs. 33-35 were substituted in Eq. 32 to calculated activation polarization in the electrodes. In addition, Eqs. 38-48 were implemented in Eqs. 36 and 37 to evaluate anode and cathode concentration polarization.

If the fuel contains H_2S, voltage drop as a result of sulfur poisoning needs to be added to the losses in Eq. 6.

3. Results and discussion

3.1 Validation

The model has been validated against some experimental data, which were not used in the development of the model. See Appendix for validation information.

3.2 Sensitivity analysis

A sensitivity analysis was conducted in order to investigate how the degradation rate is affected by the main control parameters, namely, temperature, current, and partial pressure of gases.

A conventional SOFC can operate within a temperature range of 600-900°C [61]. High operating temperatures enable SOFCs to be electrochemically active when using hydrocarbons as fuel, which eliminates the need for expensive platinum-based catalysts [62]. However, running SOFCs at temperatures above 900°C requires the use of expensive sealants that have high mechanical and chemical stability, as well as compatibility with the electrode materials. On the other hand, traditional component materials lack sufficient electrochemical activity at temperatures lower than 600°C.

In this study, current density is changed in the range of 0.2 to 1 A/cm^2 [63]. Although increasing the current density enables the use of a smaller SOFC at start of operation, which lowers capital costs, these smaller cells degrade faster, which increases maintenance costs and results in system instability.

Moreover, in the present work, it is assumed that fuel is composed of hydrogen and steam. Partial pressure of hydrogen in the fuel feed is varied from 70% to 90% of the fuel pressure.

The contour plots in Fig. 4-a, 4-d and 4-g show the sensitivity analysis results for degradation rate in the first 1000 hours of operation at 70, 80 and 90 kPa P_{H_2}, respectively. As can be seen, current density has the highest impact on the degradation rate, followed by temperature and hydrogen partial pressure, respectively.

The results over the second 1000 hours of operation (Fig. 4-b, 4-e and 4-h) show that the effects of the parameters were similar to the first 1000 hours. In other words, the degradation rate is the most sensitive to current density, with the sensitivity increasing at higher temperatures. However, degradation rate values are smaller over the second 1000 hours than the first 1000 hours, which is due to the trend of reduced degradation over time. However, the changes in degradation rate between the second and third 1000s hours of operation are not very significant. These results demonstrate that the behavior of cells changes over time, and that cells generally become more stable after approximately 1200 hours of operation.

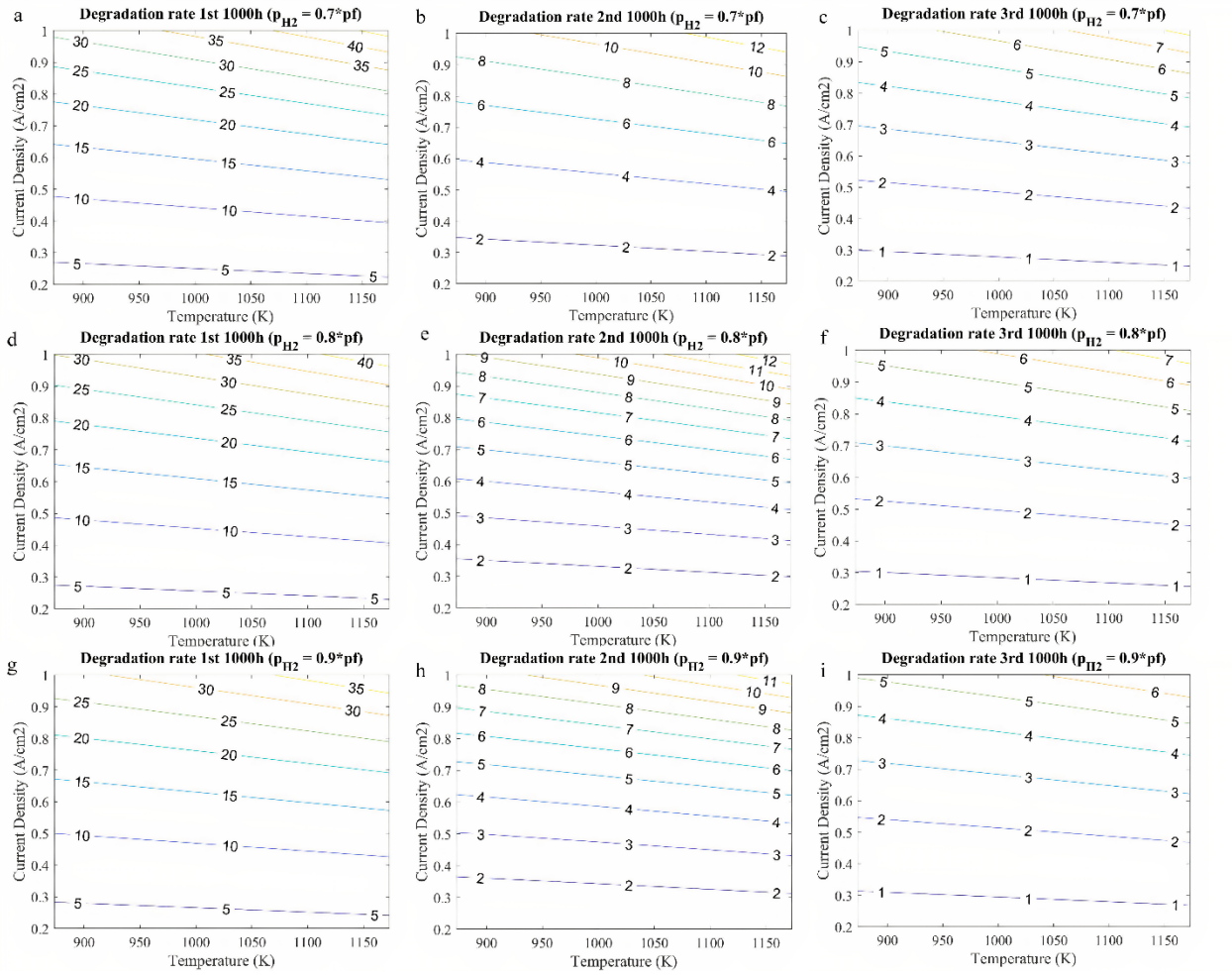

Fig. 4. Contour plots—Sensitivity analysis for degradation rate: a-c) at 70 kPa P_{H_2} for the first, second and third 1000 hours of operation, respectively; d-f) at 80 kPa P_{H_2} for the first, second and third 1000 hours of operation; and g-i) at 90 kPa P_{H_2} for the first, second and third 1000 hours of operation, respectively.

A histogram plot of the degradation rate for 6000 random samples (using Monte-Carlo random combinations of temperature, hydrogen partial pressure, and current density using the same ranges shown in Fig. 4) in different time ranges is shown in Fig. 5. As can be seen, the histograms for all three time ranges exhibit right-skewed behaviour. This asymmetric distribution shows the lower bound of the degradation rate, which is represented by the highest peak at the far left side of the histogram. However, the histogram maintains its skewed behaviour as it moves to the right, as the peaks and the entire range of degradation rates gradually become smaller with the passage of time. In addition, the height of the peak increases significantly with time as the highest peak belongs to

the third 1000 hours of operation and the smallest one belongs to the first 1000 hours of operation, while the height of the tail decreases with time.

This trend is the result of the high degradation rates that occur at the beginning of SOFC operation; the exception to this trend occurs when the SOFC is operated at a very low temperature and current density using fuel that is high in H_2. This trend of decreased deterioration over time means that the highest degradation rate also becomes less frequent after approximately 1000 hours of operation. Moreover, the value of the lowest rate, also becomes smaller over longer periods of time. As can be seen in the histogram plot, during the first 1000 hours cells might degrade up to 40 % / 1000 h when they perform at very severe conditions, while after 1000 hours of operation, degradation rates are always less than 20 % / 1000 h.

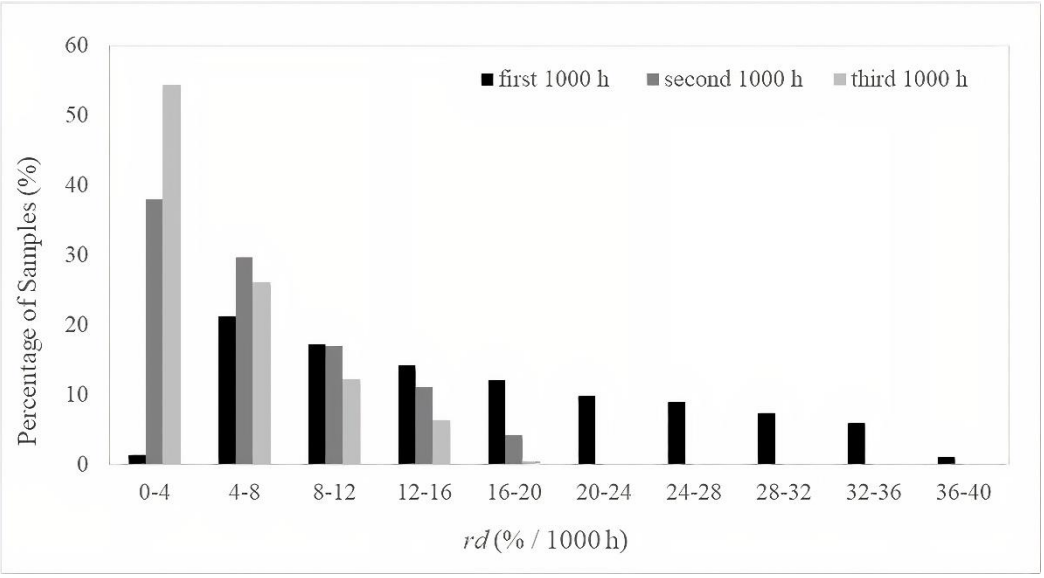

Fig. 5. Histogram plots of degradation rate percentage per 1000 hours for the first 1000 hours of operation; the second 1000 hours of operation; and the third 1000 hours of operation.

Since the focus of this work was to determine how an SOFC's operating parameters affect its performance, the sensitivity analysis is critical because it can provide specific information necessary to determine optimal operating conditions.

3.3 Application of the model to predict long-term SOFC performance

One key goal of this study was to predict the degradation rate of an SOFC over a long period of operation under different operating conditions. In order to show the variation in cell voltage over time, a simulation was run at 0.5 A/cm^2 and 750°C. The model input parameters, including physical and chemical properties of the modeled SOFCs, are given in table 2.

Table 2. Input parameters used in the degradation model of SOFC.

Parameter	Value	Parameter	Value
A	100 cm^2	$r_{YSZ,0}$	1×10^{-6} m
A_0^V	4.55×10^8 m^2/m^3	$r_{Ni,0}$	1.02×10^{-6} m
D_w	14×10^{-6} m	$\overline{Z_0}$	6.7
D_s	6.35×10^{-10} m^2 h^{-1}	φ_{an}	0.4
$E_{act,an}$	10^5 J mol^{-1}	φ_{ca}	0.5
$E_{act,ca}$	1.2×10^5 J mol^{-1}	τ_{an}	9.5
F	96485 C mol^{-1}	τ_{ca}	7.22
k_B	1.38×10^{-23} J K^{-1}	θ	15°
L_{an}	10^{-3} m	σ_{ca}	8.0×10^4 Ω^{-1} m^{-1}
L_{ca}	5×10^{-5} m	$\sigma_{0,an}$	$(3.27 \times 10^4 - 10.65$ T$) \times 10^2$ Ω^{-1} m^{-1}
L_{ele}	2×10^{-5} m	σ_{ic}	1.5×10^6 Ω^{-1} m^{-1}
L_{ic}	5×10^{-4} m	$\varepsilon_{Ni,0}$	0.4
L_{ac}	10^{-3} m	$\varepsilon_{YSZ,0}$	0.6
L_{fc}	10^{-3} m	ν_{H_2}	6.12

L_t	8×10^{-3} m	ν_{H_2O}	13.1
L_y	0.1 m	ν_{O_2}	16.3
L_z	0.1 m	ν_{N_2}	18.5
$L_{an,opt}$	3.75×10^{-4} m	γ_{an}	1.344×10^{10} A m^{-2}
$L_{ca,opt}$	7.2×10^{-4} m	γ_{ca}	2.051×10^{9} A m^{-2}
n_{ch}	10	γ	1.9 J m^{-2}
P_f	0.1 Mpa	Ω	1.09×10^{-29} m^3
P_{air}	0.1 Mpa	δ_s	2.5×10^{-10} m
P_{ref}	0.1 Mpa		
R	8.314 J mol^{-1} K^{-1}		

Fig. 6 shows that voltage degradation occurs quickly during the early hours of operation, but slows after about 1200 hours. Degradation behaviour can be explained by changes in the microstructure and properties of the cell components. As discussed in the previous section, the anode's microstructure and performance changes rapidly at first, but levels off later [45]. For instance, it was noted that Ni particles show initial rapid growth upon being exposed to gases under the SOFC's operating conditions. However, after a while, the YSZ particles slow this growth. This trend is also observed in TPB length and anode electrical conductivity, as they too are affected by number and size of Ni particles.

Fig. 6 also illustrates corresponding degradation rate of the cell. The degradation rate of the SOFC is higher in the beginning of operation and levels off as time passes. This trend indicates that, while the cells are prone to changes initially, they "mature" after about 1200 hours of operation.

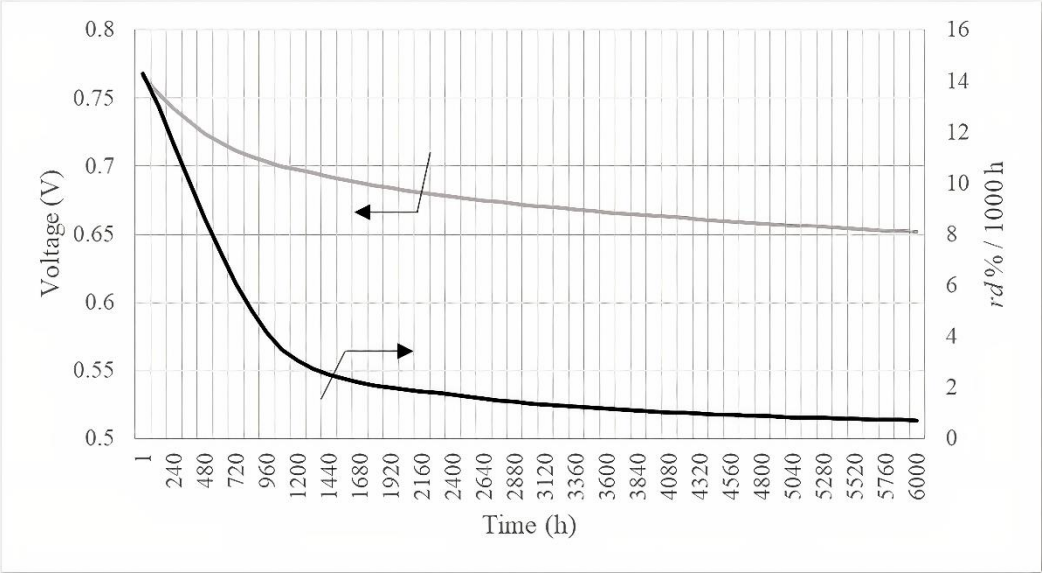

Fig. 6. Voltage profile over time, and Degradation rate percentage per 1000 hours versus time for the SOFC running at 750°C and 0.5 A/cm^2.

3.4 Effect of system operation parameters on lifetime power production

Operating parameters highly affect long-term performance of SOFCs. Depending on the operating conditions, SOFCs that perform better initially might produce less energy cumulatively over their lifetime. Fig. 7-a shows the lifetime power curves of two SOFCs that operate at different current densities but using the same fuel composition and temperature. As can be seen, the SOFC with the larger current density initially generates more power under the same conditions. However, due to the faster degradation rate associated with high current densities, the cell with the lower current density ends up providing superior power generation after about 2000 hours of operation. Comparing the cumulative energy delivered by the cells shows that after 5760 hours, cell 1 produces more energy over its lifetime.

Fig. 7-b illustrates how different the lifetime power production plots can be depending on the operating parameters. Cell 1, which runs at a higher current density and lower temperature, produces more power initially. However, after about 3000 hours, cell 1's power generation falls below that of cell 2, which is run at a lower current density and higher temperature. In fact, despite its lower operating temperature, cell 1 degrades faster due to current density's dominant effect on performance loss. The cumulative energy delivered over operation time by cell 1 exceeds that of

cell 2 after 7918 hours (at 227 kWh). The difference becomes more significant in longer periods of time as the energy generated by cell 1 over 12000 hours of operation is 335 kWh whereas, cell 2 delivers 309 kWh over the same period of time.

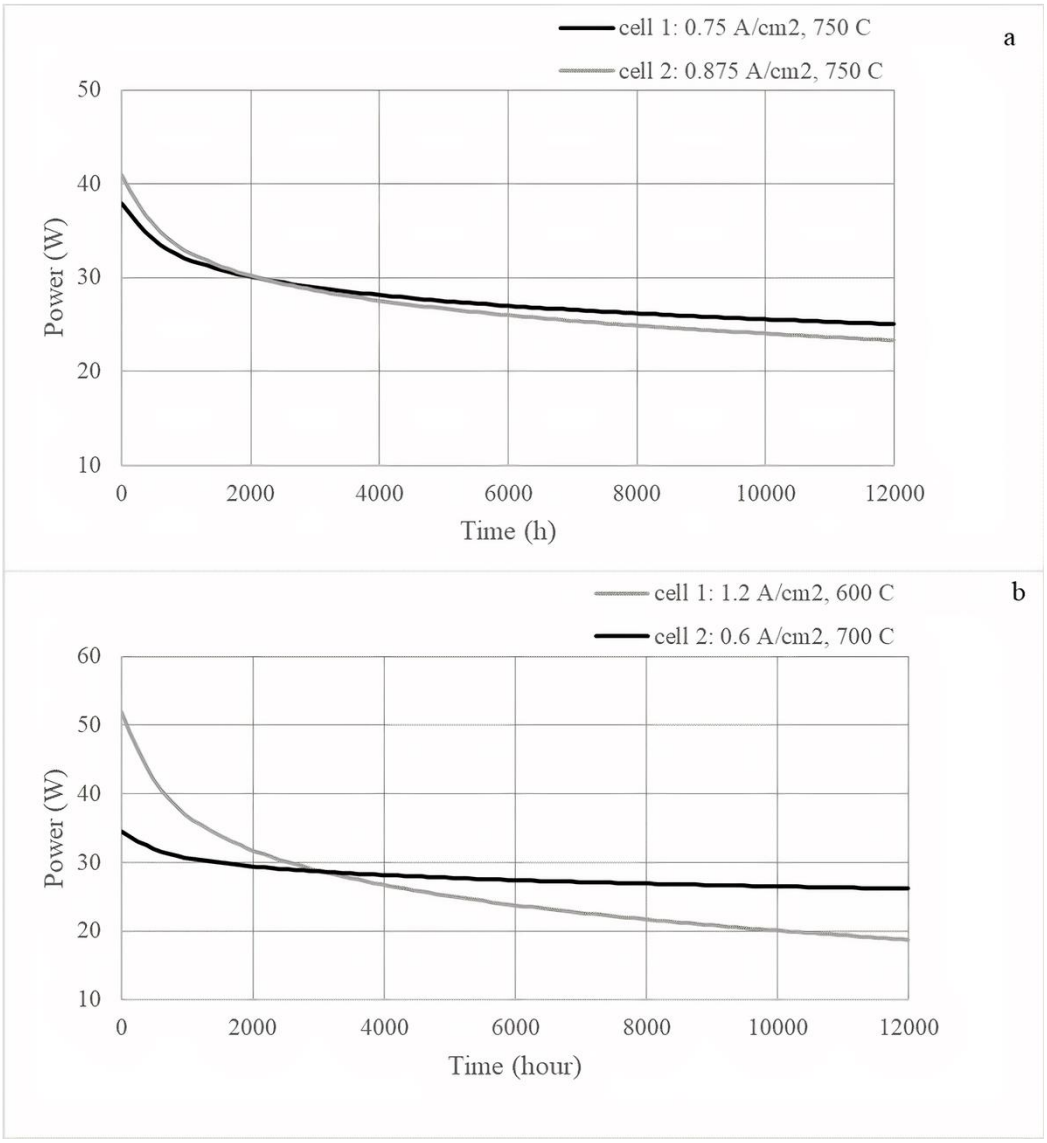

Fig. 7. a) Power profile over time for SOFCs operating at: a) 0.75 A/cm^2 and 750°C, and 0.875 A/cm^2 and 750°C; b) 1.2 A/cm^2 and 600°C, and 0.6 A/cm^2 and 700°C.

4. Future work

A detailed degradation-based system-level optimization is required to determine the optimal operating conditions for an SOFC in an ICE system. The optimal values will be highly dependent on the objective function, system level design, goals, constraints, and expected usage. If system cost is taken as the most important factor in making decisions, an optimal point will be achieved when the SOFC is able to provide a long lifespan, while still being limited in size. Applying the proposed model into an optimization framework will enable the design of a reliable system.

In addition, although the proposed degradation model was validated for 1400 hours of operation using Hagen et al.'s experimental data, some of the data-driven equations used in this research were obtained using short-term experiments [59]. Thus, these equations may not adequately represent the long-term behaviour of SOFCs. As such, more experiments are required to validate the proposed model's reliability over longer periods of time.

5. Conclusion

This paper presented a unique, cross-cutting model for long-term performance of conventional SOFCs that considers most of the common degradation phenomena in conventional SOFCs, including: coarsening and oxidation of Ni particles in the Ni-cermet anode; changes in anode pore size; deterioration in anode and electrolyte conductivity; and sulfur poisoning. By providing realistic results, this model is capable of being used to answer some important questions regarding the optimal sizing and operation of the cells for an efficient, stable performance, that previously developed models are not able to answer due to too many assumptions made for simplification. The proposed model was validated against the experimental data that was not considered in developing the model. As a result, this model can be used to predict performance of SOFCs at various operating conditions over a long period of time. This allows system designers to find the proper sizing and operation setting for SOFCs in specific ICEs. This is a critical piece of information that helps widespread commercialization of conventional SOFCs for ICEs.

The results of the sensitivity analysis can help decision makers to take control actions by showing how each key parameter impacts SOFCs long-term operation. The results illustrated that current density affects SOFCs performance significantly, while hydrogen partial pressure does not have a high impact.

This study resolved the apparent conflict in the literature about whether temperature positively or negatively affects SOFCs performance degradation. Our investigations illustrated that all these studies are correct and not actually in contradiction with each other. Instead, each study examined only specific subsets of possible degradation mechanisms and looked only at small regions of the parameter space. For example, where high temperature might cause increasing degradation of one form on one case, high temperature might actually result in lower degradation of another form in different cases. However, taking all common degradation phenomena into account holistically as a single model in the current research gave a sense of the big picture and exhibited that temperature positively correlates to degradation. In other words, the degradation rate overall increases with increasing the operating temperature.

In addition, this work highlighted the inconsistency in the literature with regard to how degradation is calculated. Instead of using the instantaneous concept of degradation rate, differing definitions of this metric are utilized across the literature which are essentially differences in the numerical finite difference approximations used with very long step sizes due to the noise in the data. This makes very different and incongruous computations of degradation rate and results in a wide range of values reported for this metric across the literature. But, with the developed model that starts from the data and utilizes an instantaneous definition, this problem is resolved and can be applied and interpreted meaningfully across all studies.

6. Acknowledgment

We thank Dr. Valentina Zaccaria for providing insights for this article and her useful suggestions. This work was supported by the Natural Sciences and Engineering Research Council of Canada [NSERC CRDPJ 509219-2017] and the Ontario Centre of Excellence [OCE 27851-2018].

7. References

[1] G. Vialetto, M. Rokni, Innovative household systems based on solid oxide fuel cells for a northern European climate, Renew. Energy. 78 (2015) 146–156. https://doi.org/10.1016/j.renene.2015.01.012.

[2] L. Barelli, G. Bidini, G. Cinti, A. Ottaviano, SOFC regulation at constant temperature: Experimental test and data regression study, Energy Convers. Manag. 117 (2016) 289–296. https://doi.org/10.1016/j.enconman.2016.03.028.

[3] V. Zaccaria, D. Tucker, A. Traverso, A distributed real-time model of degradation in a solid oxide fuel cell, part II: Analysis of fuel cell performance and potential failures, J. Power Sources. 327 (2016) 736–742. https://doi.org/10.1016/j.jpowsour.2016.01.027.

[4] T. Parhizkar, R. Roshandel, Long term performance degradation analysis and optimization of anode supported solid oxide fuel cell stacks, Energy Convers. Manag. 133 (2017) 20–30. https://doi.org/10.1016/j.enconman.2016.11.045.

[5] H. Wen, J.C. Ordonez, J.V.C. Vargas, Single solid oxide fuel cell modeling and optimization, J. Power Sources. 196 (2011) 7519–7532. https://doi.org/10.1016/j.jpowsour.2010.10.113.

[6] S. Yang, T. Chen, Y. Wang, Z. Peng, W.G. Wang, Electrochemical analysis of an anode-supported SOFC, Int. J. Electrochem. Sci. 8 (2013) 2330–2344.

[7] P. Aguiar, C.S. Adjiman, N.P. Brandon, Anode-supported intermediate temperature direct internal reforming solid oxide fuel cell. I: Model-based steady-state performance, J. Power Sources. 138 (2004) 120–136. https://doi.org/10.1016/j.jpowsour.2004.06.040.

[8] T. Parhizkar, S. Hafeznezami, Degradation based operational optimization model to improve the productivity of energy systems, case study: Solid oxide fuel cell stacks, Energy Convers. Manag. 158 (2018) 81–91. https://doi.org/10.1016/j.enconman.2017.12.045.

[9] Y.L. Liu, A. Hagen, R. Barfod, M. Chen, H.J. Wang, F.W. Poulsen, P. V. Hendriksen, Microstructural studies on degradation of interface between LSM-YSZ cathode and YSZ electrolyte in SOFCs, Solid State Ionics. 180 (2009) 1298–1304. https://doi.org/10.1016/j.ssi.2009.07.011.

[10] A. Nakajo, F. Mueller, J. Brouwer, J. Van Herle, D. Favrat, Progressive activation of degradation processes in solid oxide fuel cells stacks: Part I: Lifetime extension by optimisation of the operating conditions, J. Power Sources. 216 (2012) 449–463. https://doi.org/10.1016/j.jpowsour.2012.05.078.

[11] C.E.-S. André Weber, Julian Szász, Sebastian Dierickx, E. Ivers-Tiffée, Accelerated Lifetime Tests for SOFCs, J. Chem. Inf. Model. 53 (2013) 1689–1699.

https://doi.org/10.1017/CBO9781107415324.004.

[12] S. Taniguchi, M. Kadowaki, H. Kawamura, T. Yasuo, Y. Akiyama, Y. Miyake, T. Saitoh, Degradation phenomena in the cathode of a solid oxide fuel cell with an alloy separator, J. Power Sources. 55 (1995) 73–79. https://doi.org/10.1016/0378-7753(94)02172-Y.

[13] M.A. Abreu-Sepulveda, N.F. Harun, G. Hackett, A. Hagen, D. Tucker, Accelerated Degradation for Hardware in the Loop Simulation of Fuel Cell-Gas Turbine Hybrid System, J. Fuel Cell Sci. Technol. 12 (2015). https://doi.org/10.1115/1.4028953.

[14] T. Kim, G. Liu, M. Boaro, S.I. Lee, J.M. Vohs, R.J. Gorte, O.H. Al-Madhi, B.O. Dabbousi, A study of carbon formation and prevention in hydrocarbon-fueled SOFC, J. Power Sources. 155 (2006) 231–238. https://doi.org/10.1016/j.jpowsour.2005.05.001.

[15] D. Chen, R. Lødeng, A. Anundskås, O. Olsvik, A. Holmen, Deactivation during carbon dioxide reforming of methane over Ni catalyst: Microkinetic analysis, Chem. Eng. Sci. 56 (2001) 1371–1379. https://doi.org/10.1016/S0009-2509(00)00360-2.

[16] X. Chen, L. Zhang, E. Liu, S.P. Jiang, A fundamental study of chromium deposition and poisoning at (La 0.8Sr0.2)0.95(Mn1-xCo x)O3 ± δ (0.0≤ x ≤1.0) cathodes of solid oxide fuel cells, Int. J. Hydrogen Energy. 36 (2011) 805–821. https://doi.org/10.1016/j.ijhydene.2010.09.087.

[17] X. Chen, Y. Zhen, J. Li, S.P. Jiang, Chromium deposition and poisoning in dry and humidified air at (La0.8Sr0.2)0.9MnO3+δ cathodes of solid oxide fuel cells, Int. J. Hydrogen Energy. 35 (2010) 2477–2485. https://doi.org/10.1016/j.ijhydene.2009.12.185.

[18] S.P. Jiang, J.P. Zhang, X.G. Zheng, A comparative investigation of chromium deposition at air electrodes of solid oxide fuel cells, J. Eur. Ceram. Soc. 22 (2002) 361–373. https://doi.org/10.1016/S0955-2219(01)00280-1.

[19] Z. Cheng, J.H. Wang, Y. Choi, L. Yang, M.C. Lin, M. Liu, From Ni-YSZ to sulfur-tolerant anode materials for SOFCs: Electrochemical behavior, in situ characterization, modeling, and future perspectives, Energy Environ. Sci. 4 (2011) 4380–4409. https://doi.org/10.1039/c1ee01758f.

[20] W. Wang, C. Su, Y. Wu, R. Ran, Z. Shao, Progress in solid oxide fuel cells with nickel-

based anodes operating on methane and related fuels, Chem. Rev. 113 (2013) 8104–8151. https://doi.org/10.1021/cr300491e.

[21] T. Yoshizumi, S. Taniguchi, Y. Shiratori, K. Sasaki, Sulfur poisoning of sofcs: Voltage oscillation and Ni oxidation, J. Electrochem. Soc. 159 (2012). https://doi.org/10.1149/2.032211jes.

[22] D. Larrain, J. Van herle, D. Favrat, Simulation of SOFC stack and repeat elements including interconnect degradation and anode reoxidation risk, J. Power Sources. 161 (2006) 392–403. https://doi.org/10.1016/j.jpowsour.2006.04.151.

[23] A. Nakajo, F. Mueller, J. Brouwer, J. Van Herle, D. Favrat, Progressive activation of degradation processes in solid oxide fuel cell stacks: Part II: Spatial distribution of the degradation, J. Power Sources. 216 (2012) 434–448. https://doi.org/10.1016/j.jpowsour.2012.05.077.

[24] H. Wen, J.C. Ordonez, J.V.C. Vargas, Single solid oxide fuel cell modeling and optimization, J. Power Sources. 196 (2011) 7519–7532. https://doi.org/10.1016/j.jpowsour.2010.10.113.

[25] E.M. Ryan, W. Xu, X. Sun, M.A. Khaleel, A damage model for degradation in the electrodes of solid oxide fuel cells: Modeling the effects of sulfur and antimony in the anode, J. Power Sources. 210 (2012) 233–242. https://doi.org/10.1016/j.jpowsour.2012.02.091.

[26] J.B. Hansen, Correlating sulfur poisoning of SOFC nickel anodes by a temkin isotherm, Electrochem. Solid-State Lett. 11 (2008) 178–180. https://doi.org/10.1149/1.2960521.

[27] D. Tucker, M. Abreu-Sepulveda, N.F. Harun, SOFC lifetime assessment in gas turbine hybrid power systems, J. Fuel Cell Sci. Technol. 11 (2014). https://doi.org/10.1115/1.4028158.

[28] W.G. Coors, J.R. O'Brien, J.T. White, Conductivity degradation of NiO-containing 8YSZ and 10YSZ electrolyte during reduction, Solid State Ionics. 180 (2009) 246–251. https://doi.org/10.1016/j.ssi.2008.12.004.

[29] S. Gao, J. Li, Z. Lin, Theoretical model for surface diffusion driven Ni-particle

agglomeration in anode of solid oxide fuel cell, J. Power Sources. 255 (2014) 144–150. https://doi.org/10.1016/j.jpowsour.2014.01.033.

[30] J.P. Neidhardt, D.N. Fronczek, T. Jahnke, T. Danner, B. Horstmann, W.G. Bessler, A flexible framework for modeling multiple solid, liquid and gaseous phases in batteries and fuel cells, J. Electrochem. Soc. 159 (2012) 1528–1542. https://doi.org/10.1149/2.023209jes.

[31] E. Hardjo, D. Monder, K. Karan, Numerical modeling of nickel-impregnated porous YSZ-supported anodes and comparison to conventional composite Ni-YSZ electrodes, ECS Trans. 35 (2011) 1823–1832. https://doi.org/10.1149/1.3570171.

[32] E.F. Hardjo, D.S. Monder, K. Karan, An effective property model for infiltrated electrodes in solid oxide fuel cells, J. Electrochem. Soc. 161 (2014). https://doi.org/10.1149/2.036401jes.

[33] J. Divisek, R. Wilkenhöner, Y. Volfkovich, Structure investigations of SOFC anode cermets Part I: Porosity investigations, J. Appl. Electrochem. 29 (1999) 153–163. https://doi.org/10.1023/A:1003420815623.

[34] T. Yoshizumi, C. Uryu, T. Oshima, Y. Shiratori, K. Ito, K. Sasaki, Sulfur poisoning of SOFCs: Dependence on operational parameters, ECS Trans. 35 (2011) 1717–1725. https://doi.org/10.1149/1.3570159.

[35] A. Hagen, G.B. Johnson, P. Hjalmarsson, Electrochemical evaluation of sulfur poisoning in a methane-fuelled solid oxide fuel cell: Effect of current density and sulfur concentration, J. Power Sources. 272 (2014) 776–785. https://doi.org/10.1016/j.jpowsour.2014.08.125.

[36] L. Aguilar, S. Zha, Z. Cheng, J. Winnick, M. Liu, A solid oxide fuel cell operating on hydrogen sulfide (H2S) and sulfur-containing fuels, J. Power Sources. 135 (2004) 17–24. https://doi.org/10.1016/j.jpowsour.2004.03.061.

[37] H. Langnickel, A. Hagen, New methodology of studying H2S poisoning effects on SOFC’s fueled by carbon containing fuels like biogas, ECS Trans. 91 (2019) 511–521. https://doi.org/10.1149/09101.0511ecst.

[38] M.C. Williams, J.P. Strakey, W.A. Surdoval, U. S. DOE solid oxide fuel cells: Technical advances, Proc. - Electrochem. Soc. PV 2005-07 (2005) 20–31. https://doi.org/10.1149/200507.0020pv.

[39] T.A. Adams, J. Nease, D. Tucker, P.I. Barton, Energy conversion with solid oxide fuel cell systems: A review of concepts and outlooks for the short- and long-term, Ind. Eng. Chem. Res. 52 (2013) 3089–3111. https://doi.org/10.1021/ie300996r.

[40] G. Chiodelli, L. Malavasi, Electrochemical open circuit voltage (OCV) characterization of SOFC materials, Ionics (Kiel). 19 (2013) 1135–1144. https://doi.org/10.1007/s11581-013-0843-z.

[41] A. Faes, A. Hessler-Wyser, D. Presvytes, C.G. Vayenas, J. Vanherle, Nickel-zirconia anode degradation and triple phase boundary quantification from microstructural analysis, Fuel Cells. 9 (2009) 841–851. https://doi.org/10.1002/fuce.200800147.

[42] P. Tanasini, M. Cannarozzo, P. Costamagna, A. Faes, J. Van Herle, A. Hessler-Wyser, C. Comninellis, Experimental and theoretical investigation of degradation mechanisms by particle coarsening in sofc electrodes, Fuel Cells. 9 (2009) 740–752. https://doi.org/10.1002/fuce.200800192.

[43] N. Laosiripojana, W. Wiyaratn, W. Kiatkittipong, A. Arpornwichanop, A. Soottitantawat, S. Assabumrungrat, R Eviews on S Olid O Xide, 13 (2009) 65–83. https://doi.org/10.4186/ej.2009.13.1.65.

[44] W. Zhu, D. Ding, C. Xia, Enhancement in three-phase boundary of SOFC electrodes by an ion impregnation method: A modeling comparison, Electrochem. Solid-State Lett. 11 (2008) 83–86. https://doi.org/10.1149/1.2895009.

[45] J. Chen, A. Bertei, E. Ruiz-Trejo, A. Atkinson, N.P. Brandon, Characterization of degradation in nickel impregnated scandia-stabilize zirconia electrodes during isothermal annealing, J. Electrochem. Soc. 164 (2017) F935–F943. https://doi.org/10.1149/2.0821709jes.

[46] T. Klemensø, K. Thydén, M. Chen, H.J. Wang, Stability of Ni-yttria stabilized zirconia anodes based on Ni-impregnation, J. Power Sources. 195 (2010) 7295–7301.

https://doi.org/10.1016/j.jpowsour.2010.05.047.

[47] M.Cs.-K.Ml. T, No Title, n.d. https://doi.org/https://doi.org/10.1016/C2013-0-16429-X.

[48] P. Costamagna, K. Honegger, Modeling of solid oxide heat exchanger integrated stacks and simulation at high fuel utilization, J. Electrochem. Soc. 145 (1998) 3995–4007. https://doi.org/10.1149/1.1838904.

[49] S.H. Chan, K.A. Khor, Z.T. Xia, Complete polarization model of a solid oxide fuel cell and its sensitivity to the change of cell component thickness, J. Power Sources. 93 (2001) 130–140. https://doi.org/10.1016/S0378-7753(00)00556-5.

[50] S. Chapman, T.G. Cowling, D. Park, The Mathematical Theory of Non-Uniform Gases, Am. J. Phys. 30 (1962) 389–389. https://doi.org/10.1119/1.1942035.

[51] J.H. Arnold, Studies in Diffusion: I—Estimation of Diffusivities in Gaseous Systems, Ind. Eng. Chem. 22 (1930) 1091–1095. https://doi.org/10.1021/ie50250a023.

[52] E.R. Gilliland, Diffusion Coefficients in Gaseous Systems, Ind. Eng. Chem. 26 (1934) 681–685. https://doi.org/10.1021/ie50294a020.

[53] E.N. Fuller, K. Ensley, J.C. Giddings, Diffusion of halogenated hydrocarbons in helium. The effect of structure on collision cross sections, J. Phys. Chem. 73 (1969) 3679–3685. https://doi.org/10.1021/j100845a020.

[54] Y. Matsuzaki, I. Yasuda, Poisoning effect of sulfur-containing impurity gas on a SOFC anode: Part I. Dependence on temperature, time, and impurity concentration, Solid State Ionics. 132 (2000) 261–269. https://doi.org/10.1016/s0167-2738(00)00653-6.

[55] J.F.B. Rasmussen, A. Hagen, The effect of H2S on the performance of Ni-YSZ anodes in solid oxide fuel cells, J. Power Sources. 191 (2009) 534–541. https://doi.org/10.1016/j.jpowsour.2009.02.001.

[56] J.R.R.-N. and S.R. Ib Alstrup, High Temperature Hydrogen Sulfide Chemisorption on Nickel Catalysts, Appl. Catal. 1 (1981) 303–314.

[57] S. Zha, Z. Cheng, M. Liu, Sulfur poisoning and regeneration of ni-based anodes in solid oxide fuel cells, J. Electrochem. Soc. 154 (2007) 201–206.

https://doi.org/10.1149/1.2404779.

[58] Z. Cheng, S. Zha, M. Liu, Influence of cell voltage and current on sulfur poisoning behavior of solid oxide fuel cells, J. Power Sources. 172 (2007) 688–693. https://doi.org/10.1016/j.jpowsour.2007.07.052.

[59] A. Hagen, R. Barfod, P.V. Hendriksen, Y.L. Liu, S. Ramousse, Degradation of anode supported SOFCs as a function of temperature and current load, J. Electrochem. Soc. 153 (2006) 1165–1171. https://doi.org/10.1149/1.2193400.

[60] R.S. Gemmen, M.C. Williams, K. Gerdes, Degradation measurement and analysis for cells and stacks, J. Power Sources. 184 (2008) 251–259. https://doi.org/10.1016/j.jpowsour.2008.06.047.

[61] A.A. Kulikovsky, Analytical modeling of fuel cells, in: 2010: pp. 1–33.

[62] D. Uttamchandani, Wireless MEMS networks and apllications, in: 2016: p. 40.

[63] M. Lang, C. Bohn, M. Henke, G. Schiller, C. Willich, F. Hauler, Understanding the current-voltage behavior of high temperature solid oxide fuel cell stacks, J. Electrochem. Soc. 164 (2017) F1460–F1470. https://doi.org/10.1149/2.1541713jes.